Molecular Dynamics of Polyisoprene/Polystyrene Oligomer Blends: The role of self-concentration and fluctuations on blend dynamics

Vagelis A. Harmandaris and Manolis Doxastakis

Molecular Dynamics of Polyisoprene/Polystyrene Oligomer Blends: The role of self-concentration and fluctuations on blend dynamics

Vagelis Harmandaris[1, a)] and Manolis Doxastakis[2, b)]

[1)] *Department of Applied Mathematics, University of Crete, and IACM FORTH GR-71110 Heraklion, Greece*

[2)] *Department of Chemical and Biomolecular Engineering, University of Houston, Houston, Texas*

(Dated: 7 March 2013)

The effect of self-concentration and intermolecular packing on the dynamics of polyisoprene (PI)/polystyrene (PS) blends is examined by extensive atomistic simulations. Direct information on local structure of the blend system allows a quantitative calculation of self- and effective composition terms at various length scales that are introduced to proposed models of blend dynamics. Through a detailed statistical analysis, the full distribution of relaxation times associated with reorienation of carbon-hydrogen bonds was extracted and compared to literature experimental data. A direct relation between relaxation times and local effective composition is found. Following an implementation of a model involving local composition as well as concentration fluctuations the relevant length scales characterizing the segmental dynamics of both components were critically examined. For PI the distribution of times becomes narrower for the system with the lowest PS content and then broadens as more PS is added. This is in contrast to the slow component (PS), where an extreme breadth is found for relaxation times in the 25/75 system prior to narrowing as we increase PI concentration. The chain dynamics was directly quantified by diffusion coefficients as well as the terminal (maximum) relaxation time of each component in the mixed state. Strong coupling between the friction coefficients of the two components was predicted that leads to very similar chain dynamics for PI and PS, particularly for high concentrations of PI. We anticipate this finding to the rather short oligomers (below the Rouse regime) studied here as well as to the rather similar size of PI and PS chains. The ratio of the terminal to the segmental relaxation time, $\tau_{\mathrm{term}}/\tau_{\mathrm{seg,c}}$, presents a clear qualitative difference for the constituents: for PS the above ratio is almost independent of blend composition and very similar to the pure state. In contrast, for PI this ratio depends strongly on the composition of the blend; i.e. the terminal relaxation time of PI increases more than its segmental relaxation time, as the concentration of PS increases, resulting into a larger terminal/segmental ratio. We explain this disparity, based on the different length scales characterizing dynamics. The relevant length for the segmental dynamics of PI is about 0.4-0.6 nm, smaller than chain dimensions which are expected to characterize terminal dynamics, whereas for PS associated length scales are similar (about 0.7-1.0 nm) rendering a uniform change with mixing.

[a)]Electronic mail: vagelis@tem.uoc.gr

[b)]Electronic mail: edoxastakis@uh.edu

I. INTRODUCTION

The dynamics of polymer mixtures remains an area of intense research for nearly two decades due to their complex rheological behavior. It is well established that even thermodynamically miscible blends, such as polyisoprene (PI)/1,2 polybutadiene (PVE) can retain distinct individual mobilities in the mixed state that are separate from the pure components.[1] A critical parameter in the observed behavior is the dynamic asymmetry, controlled by the difference in the glass transition temperatures (T_g) of the constituent homopolymers. Devising simple, efficient and general models that interpret the observed dynamic heterogeneity and formulate mixing rules is a critical step towards choosing appropriate processing conditions in practical industrial applications. However, despite continuous development for more than a decade, this remains a challenging task with several open questions pertaining to linking molecular details to model parameters. Excellent reviews in the literature provide a thorough background of accumulated knowledge[2,3] therefore we focus in this introduction on aspects that motivated the current study.

Several models combine concentration fluctuations and contributions from chain connectivity to provide a framework that rationalizes the observed experimental behavior. Concentration fluctuations are expected to be present in mixtures and depending on their lifetime they can promote a distribution of segmental decorrelation rates. This view of polymer blend dynamics was proposed by Zetsche and Fischer[4] and further developed in subsequent studies that extended the concept of concentration fluctuations beyond a Gaussian form, to capture experimental and simulation data.[5–15] Some of the aforementioned studies added the effect of self-concentration, first introduced by Chung *et al.*[16] and further elaborated by the Lodge-McLeish (LM) model.[17] According to this concept, each segment of a specific component A is experiencing an environment that is enriched to A due to chain connectivity.[16] To create a quantitative formalism, it is necessary to select an appropriate lengthscale over which self-concentration and fluctuations in composition control segmental dynamics. The success of these theoretical models to capture qualitatively experimental findings, fueled extensive studies aiming to offer a quantitative prediction of dynamics in polymer blends.

He *et al.* examined extensively the segmental and terminal dynamics of polyisoprene (PI) /polystyrene (PS) oligomers.[18] While homogeneous terminal dynamics were probed, segmental relaxation rates were significantly different. By refinement of self-concentration

terms ϕ_{self} the LM model provided a reasonable description of experimental data. However the actual values (0.33 ± 0.05 for PI and 0.42 ± 0.07 for PS) differed from the anticipated 0.45 and 0.27 based on a direct application the original LM model. As described by the authors, the actual values are largely dependent on the length scale (volume) over which the self-concentration term is evaluated. This volume should be in the order of l_K^3 where l_K is the Kuhn length of the polymer segment whose dynamics are examined. Shenogin *et al.*[19] supported that a single correlation length that is composition-independent can reproduce experimental data; however concentration fluctuations need to be incorporated in the LM model. Using both self-correlation terms and fluctuations, a distribution of effective compositions $p(\phi_{\text{eff}})$ can be turned to a distribution of segmental times $p(\log \tau)$ given a specific correlation length. By iteratively refining predictions of the model to experimental data, short length scales were predicted for PI in the range of 4-10 Å. Nevertheless, as stated by the authors, the actual values are quite sensitive to the analysis procedure to have any molecular significance. We add, that the complete distribution of times is required to obtain an accurate description since as shown by Kumar et al.[20] mean times and peaks of the distribution can both be affected by local composition and fluctuations. It is important to add in our introduction a subsequent study by Liu *et al.*, employing bead-spring models that demonstrated that even the self-concentration term should be described by a non-Gaussian distribution of concentrations rather than a constant value.[21] This feature is particularly important for dilute blends.

Simple lattice models can provide valuable qualitative aspects of the correlation between composition and dynamics of model polymer blends. Using such models Colby and Lipson[22] analyzed data from dielectric experiments of PI/PVE blends to show that, by accounting for the relatively strong composition dependence of the blend T_g, it is possible to model the dielectric relaxation spectrum by considering concentration fluctuations at the scale of the Kuhn length; the latter is both composition and temperature independent. More recently White and Lipson,[23] using a simple lattice-based equation of state, examined correlations between the difference of pure component energy parameters and their bulk miscibility, using various experimental data for blends exhibiting both upper and lower critical solution temperature. Finally, recently Colmenero, Richter and co-workers in a series of papers[24–26] studied the effect of blending on dynamics using dielectric spectroscopy, neutron scattering and simulations with bead-spring models. Among other systems they studied the dynamics

PI/poly(tert-butylstyrene)(PtBS) miscible blends. They found that as the concentration of the higher-T_g component PtBS increases, the dielectric response of PI becomes slower and there is a gradual broadening of both low- and high- frequency tails of the normal mode relaxation of PI.

For miscible oligomer mixtures, dynamics are today directly accessible by fully atomistic molecular dynamics simulations. Using such detailed models, Faller demonstrated that heterogeneous segmental dynamics are present in the PI/PS mixture associated with length-scales up to 1.3 nm.[27] Maranas and co-workers[2,28] compared the dynamics of a poly(ethylene oxide)(PEO) and poly(methyl methacrylate)(PMMA) with that of a diblock copolymer of the same overall composition. As shown, differences in the intermolecular packing of the blend and the copolymer leads to variations in composition defined over local length scales.

In this study, we examine whether the dynamics in PI/PS oligomer blends as described by atomistic simulations, can be predicted by employing the concept of self-concentration combined with composition fluctuations which lead to a distribution of relaxation times. We rely on extensive analysis of decorrelation rates as well as the ability to create long trajectories that provide sufficient sampling both for local as well as terminal dynamics. In the next section we describe the models and the overall simulation methodology followed. In Section 3 we present results from the atomistic simulations of the polymer blends. We analyze the structure, the composition and the dynamics of the model systems. Finally, our findings and conclusions are summarized in Section 4.

II. MODELS AND METHODOLOGY

A. Polyisoprene Model

Polyisoprene (PI) is modeled based on a fully atomistic description that is described in the literature and was previously employed to study PI/PS.[27,29,30] We verified that the conformational and thermodynamic properties are reproduced faithfully using a series of simulations ranging from an 8-mer to a 24-mer at 413K. Extrapolation to high-molecular weight resulted to a specific volume of 1.175 cm^3/g which is in excellent agreement to available estimates of 1.183-1.196 cm^3/g at this temperature.[31,32] Conformational properties were also consistent with data in the literature; extrapolating to infinity the characteristic

ratio is expected to be in the range of 4.5-4.8. However, for the 12-mer employed in this study, a value of ≈ 3.8 was extracted (using an average square bond length $l^2 \approx 2.18$ Å^2). We estimate that a monomer adds approximately 4.58 Å to the contour length which will result to a maximum extension for the 12-mer of 53.1 Å and a Kuhn length segment of 7.5 Å; a value that is somewhat lower than the reported 8.2 Å for high molecular weight polyisoprene.[33]

B. Polystyrene Model

Polystyrene (PS) atactic oligomers (10mer) are also modeled using an all-atom model, where hydrogens and carbons are treated explicitly. All bond lengths were kept rigid whereas a harmonic potential was used to describe bond angle bending. Standard torsional potentials were used to describe rotations along bonds in the aliphatic backbone. Parameters of the barriers for the rotation of polystyrene backbone dihedral angles were calculated from ab initio calculations on polystyrene fragments. Non-bonded interactions were described by pairwise-additive Lennard-Jones potentials. The model included partial charges on the carbon and hydrogen atoms of the phenyl groups that reproduce the electric quadropole moment of the benzene molecule. Additional details of the model are reported in the literature.[34] The chain dimensions as well as the structure of PS bulk systems are in good agreement with available experimental data.[35,36] It is important to note that this model predicts slower PS dynamics (a factor of about 4-5), compared to experimental data from dielectric spectroscopy.[37] For PS the extracted value for the characteristic ratio is about 5.0, lower than the high molecular value of about 9.8 as reported in previous studies.[38] This value results to a Kuhn segment $l_k \approx 7.65$ Å, for the PS oligomers studied here, smaller than the value of 15.0 Å for high molecular weight PS. In previous works we have studied extensively the PS model predictions for structure, dimensions and dynamics of PS systems as a function of molecular weight.[39,40]

C. Simulation Methodology

Simulations were performed with the molecular dynamics software Gromacs 4.5.5[41,42] in the NPT ensemble maintaining a pressure of 1 bar at four different temperatures T: 413, 443,

TABLE I. Details of systems studied. The weight fraction is used to name each system studied. The number fraction of the corresponding component for each system is provided in parenthesis.

Polyisoprene (wt%)	100	75	50	25	0
12-mer *cis*-1,4 PI chains (MW=819 g/mol)	72	46	32	17	0
	(1)	(0.79)	(0.56)	(0.29)	(1)
10-mer atactic PS chains (MW=1043.5 g/mol)	0	12	25	40	56
	(0)	(0.21)	(0.44)	(0.71)	(1)

473 and 503 K. Pressure P was maintained with the Berendsen thermostat with $\tau = 0.1$ ps while temperature control was introduced through the stochastic velocity rescaling scheme.[43]

A twin cut-off scheme was applied with full van der Waals interactions up to 0.9 nm and a smooth switch to zero at 1 nm. Electrostatics were calculated with a particle mesh Ewald method.[44] All bonds were kept constant using the P-Lincs algorithm[45] which allowed a timestep of 1 fs. For mixtures at least 200 ns trajectories were generated, far beyond the relaxation time of these oligomers. For pure PI, 20 ns were sufficient to accumulate good statistics while for pure PS simulations were extended to 400 ns due to slow dynamics of this component in the pure state. In addition to these long simulations several 200 ps trajectories were created to extract the short-time dynamic behavior of the systems with configurations recorded at time intervals of 0.1 or 0.2 ps. To be able to merge consistently results from short- and long-trajectories we employed the following strategy: simulation snapshots from long runs separated by 10 ns were utilized as starting points (with the stored positions and velocities) for the short simulations. Results from the last (i.e. autocorrelation functions) were averaged out with the outcome describing faithfully the initial decay of curves generated by long-time trajectories where time-frames were more sparsely recorded (i.e. every 100 ps). We should also note here that using the Flory-Huggins interaction parameter for PI and PS we can calculate the critical point of our blend. Indeed, using a temperature dependent χ factor ($\chi = -0.07 + 63/T$)[6] the critical point of our PI/PS blend is at T_c=332 K, ϕ_c=0.49. The temperature range of our simulations (413-503 K) is well above T_c.

III. RESULTS AND DISCUSSION

A. Density of systems

We begin our discussion by first examining macroscopic properties of the oligomer mixtures studied. PS, even as an oligomer, maintains a significantly higher density than its mixtures with PI as shown in Fig. 1a. Higher temperatures uniformly increase the overall density. For our discussion, it is important to emphasize that while mixing alters mass density, in terms of atom number density the effect is minimal; this originates directly from the higher packing of PS chains. As can been seen in Fig. 1b, the number of atoms/interaction sites per nm^3 remains practically constant with concentration for higher temperatures (473K and 503K) while small changes are observed at lower temperatures (443K and 413K).

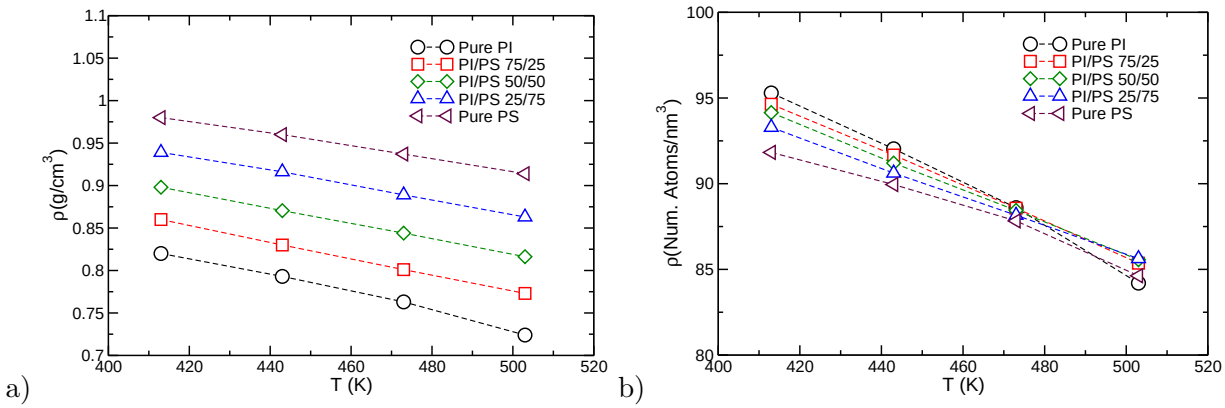

FIG. 1. a) Density of the mixtures at $P = 1$ atm as predicted with the models studied. b) Number density of atoms at $P = 1$ atm; notice that mixing does not alter significantly the number of atoms per volume while small changes are induced by altering temperature T.

B. Structure and Self-concentration

We first discuss how components distribute within the oligomer melts. The LM model employs local volume fractions to correlate compositions around a polymer segment to the observed dynamic behavior. Calculation of volume fractions from the simulation data is not straightforward. Alternatively, a fraction of atoms can be employed within a specific volume. In general, for a blend of A and B we can quantify self- and effective concentrations

using:

$$\phi_{\mathrm{self,i}}(r) = \frac{N_i^{\mathrm{intra}}(r)}{N_A(r) + N_B(r)} \qquad \phi_{\mathrm{eff,i}}(r) = \frac{N_i(r)}{N_A(r) + N_B(r)} \tag{1}$$

where $i = A$ or B, and the self- (and effective) concentrations $\phi_{\mathrm{self,i}}(r)$, ($\phi_{\mathrm{eff,i}}(r)$) of i are calculated by the number fraction of intramolecular neighbors $N_i^{\mathrm{intra}}(r)$ (and total neighbors $N_i(r)$) relative to the total $N_A(r) + N_B(r)$ contained within a sphere of radius r.[28] While we anticipate minimal changes of the self-concentration term, the above definition presents a subtle decrease as we decrease T for pure components due to higher increases in the denominator $N_A(r) + N_B(r)$ with lowering T; closer packing of the chains will reduce the self-fraction. Here we should also note that we could use mass instead of number fractions. In that case, results are similar and the whole discussion remains unchanged.

To provide a more transparent examination of our results we selected to work first with absolute number densities of atoms within specific volumes. Figs. 2a) and b) present the radial number distribution function (RDF) with a frame of reference a PI or a PS atom for the pure components at 443 K (unnormalized). Notice that intermolecular packing is significantly different with interchain neighbors rising at a faster pace in PI; a similar trend carries over to partial RDFs in mixtures as reported in the past.[27] To examine how self-concentration varies with distance, a cumulative number of atoms within a sphere r needs to be calculated as shown in Figs. 2c, d. As expected, these curves are smoother than RDFs. We evaluated the ratio of the cumulative concentrations to calculate the term $\phi_{\mathrm{self,i}}(r)$ solely for pure components, as shown in the inset of Figs. 2c, d. The LM model introduces a cooperative volume that is in the order of l_k^3, or $v_{k,\mathrm{PI}} \propto 0.422$ nm^3 and $v_{k,\mathrm{PS}} \propto 0.447$ nm^3 for PI and PS respectively using concepts of cubic volumes; the exact value for an appropriate spherical volume to be selected is often determined through laborious treatment of experimental data employing necessary approximations.

Without *a priori* knowledge on dynamics, one approach would be to set these volumes equal to the above values and calculate a radius that provides the same spherical volume, $r = 0.5 * l_k * (6/\pi)^{1/3}$ which results to 4.65 Å for PI and 4.74 Å for PS, respectively. These values will provide self-terms that are very high and in disagreement with the optimum values reported by He *et al.* ($\phi_{\mathrm{self,PI}}(r) = 0.33 \pm 0.05$ and $\phi_{\mathrm{self,PS}}(r) = 0.42 \pm 0.07$).[18] While the experimental parameters refer to mixtures, as we will see below, mixing can not justify such large differences. In addition, the LM predicts a self-concentration that should be lower for PS compared to PI. Similar very high values for self-terms can be extracted if we select

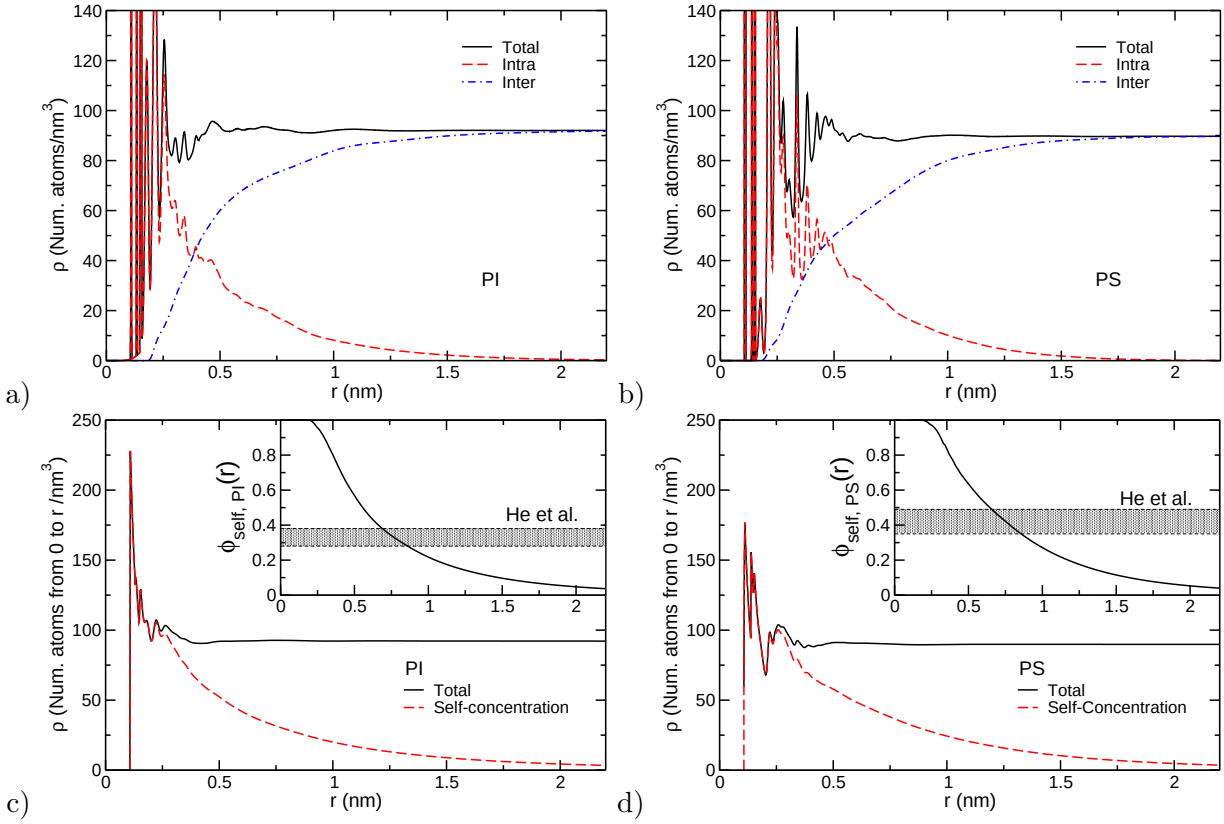

FIG. 2. a) Radial number density as a function of distance for PI at 443K. b) Radial number density as a function of distance for PS at 443K. c) Number density of atoms within a sphere r starting from a PI atom, for pure PI at 443K. The inset provides the ratio $\phi_{\mathrm{self,i}}(r)$. d) Number density of atoms within a sphere r starting from a PS atom, for pure PS at 443K. The inset provides the ratio $\phi_{\mathrm{self,i}}(r)$.

$r = l_k/2$ as performed by Sacristan *et al.*.[28] Since the model is phenomenological and the constant of proportionality is rather arbitrary, we could also select as radius of the sphere the full Kuhn length l_k and the corresponding volumes equal to $4\pi l_k^3/3$. Under this assumption, for pure melts, $\phi_{\mathrm{self,PI}}(r) \approx 0.37$ and $\phi_{\mathrm{self,PS}}(r) \approx 0.40$. All these arguments though neglect fluctuations and as stated by Shenogin et al. the whole distribution of $\phi_{\mathrm{self}}(r)$ at a specific distance should be considered rather than the mean value.[19] Prior to examine these features we need to interrogate potential changes with temperature and composition.

Figs. 3a and b, present the radial density of atoms decomposed to individual contributions for a shell from r to $r + dr$ starting from a PI or a PS atom respectively. It is clearly

observed that locally, concentrations are enriched on the component that serves as a point of reference due to the self-concentration term. To quantify the relative contribution of this term, for a spherical volume extending from an atom to r, the cumulative amounts are calculated over the total volume as performed previously for pure components. Figs. 3c and d present such graphs for the 50/50 blend at 443K. As it is observed, the local effective concentration calculated directly from the simulation is higher than the bulk and converges to the latter value as the self-concentration term approaches zero. Notice again, that since this calculation includes a cumulative amount, the range over which this deviation persists is further away than the point where a shell dv reaches the average composition. This is anticipated given that the rich in intramolecular neighbors envirnoment needs to be diluted extensively to asymptotically reach the average fraction. The inset in these plots, presents again the normalized fraction of self-concentration as calculated by Eq. 1. As it is evident, no significant deviation from the pure components exists.

We can also calculate the fraction of the self- to total concentration (in Figs. 3c, d) to obtain the normalized effective concentration of a component directly from the simulation and compare to the approach employed by the LM model . This is shown explicitly in Figs. 3e and f. According to the LM model, the effective concentration is calculated given the self-term, using the formula:

$$\begin{aligned} \phi_{\text{eff, A}} &= \phi_{\text{self, A}} + (1 - \phi_{\text{self, A}})\phi_A \\ \phi_{\text{eff, B}} &= \phi_{\text{self, B}} + (1 - \phi_{\text{self, B}})\phi_B \end{aligned} \tag{2}$$

where ϕ_A and ϕ_B are the bulk volume fractions of A and B respectively. Lipson and Milner[46] proposed a modification of the above expression that resulted in a self-consistent definition (SCLM):

$$\begin{aligned} \phi_{\text{eff, A}} &= \phi_{\text{self, A}} + (1 - \phi_{\text{self, A}})p \\ \phi_{\text{eff, B}} &= \phi_{\text{self, B}} + (1 - \phi_{\text{self, B}})(1 - p) \end{aligned} \tag{3}$$

where p:

$$p = \frac{(1 - \phi_{\text{self, A}})\phi_A}{(1 - \phi_{\text{self, A}})\phi_A + (1 - \phi_{\text{self, B}})\phi_B} \tag{4}$$

In both models, $\phi_{\text{self, i}}$ needs to be estimated. In the data above, direct calculation of $\phi_{\text{self, i}}(r)$ allows a first test of the above combination rules given the bulk ϕ_i reported in Table I. As

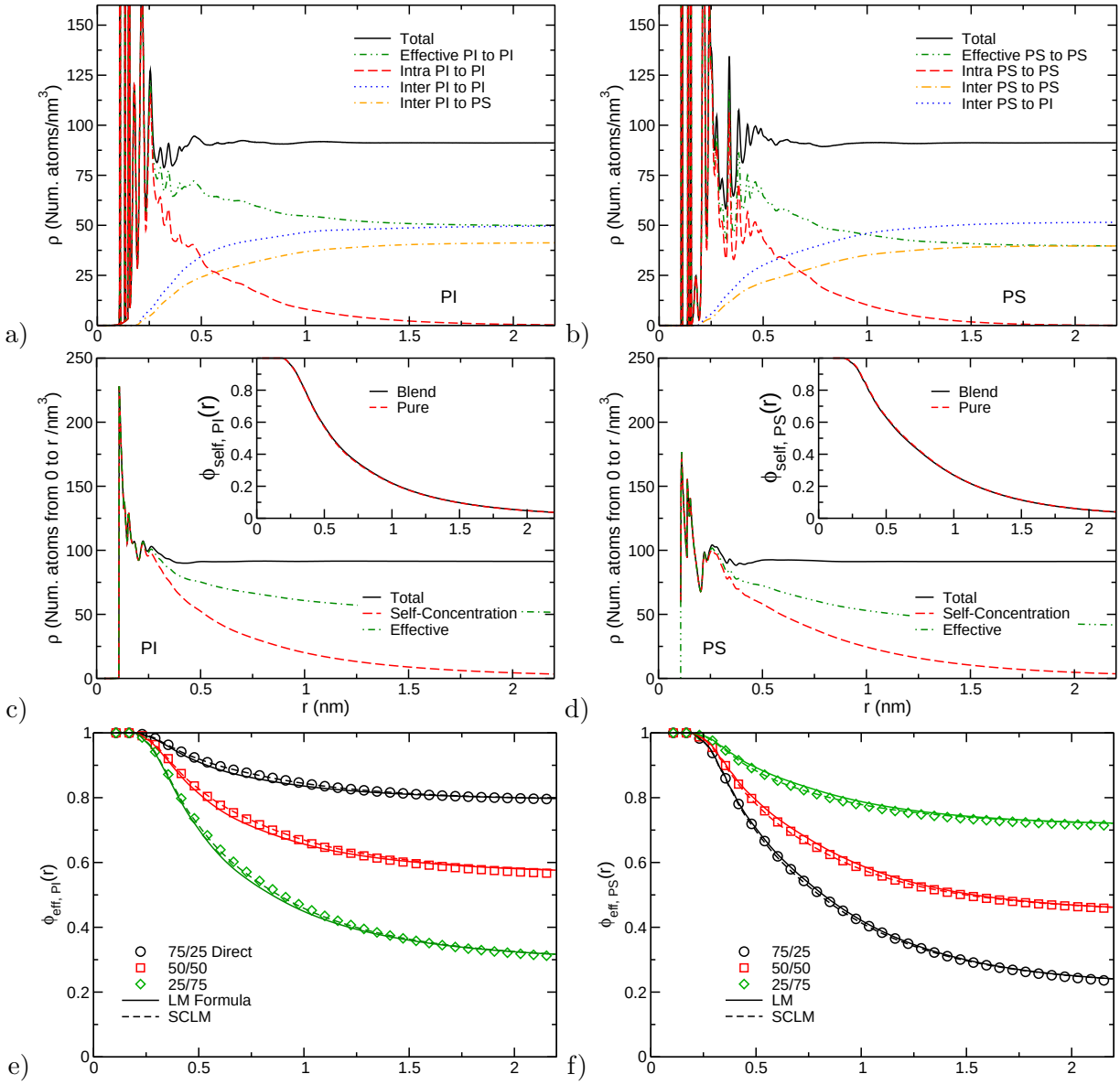

FIG. 3. a) Radial number density as a function of distance from a PI atom for a 50 wt% PI blend. b) Radial number density as a function of distance from a PS atom for a 50 wt% PI blend. c) Number density of atoms within a sphere r starting from a PI atom. The inset provides the ratio $\phi_{\mathrm{self,i}}(r)$ compared to pure PI. d) Number density of atoms within a sphere r starting from a PS atom. The inset provides the ratio $\phi_{\mathrm{self,i}}(r)$ compared to pure PS. e) and f) Effective PI (PS) fraction around a PI (PS) atom. In all cases $T = 443$K.

observed in Figs. 3 by employing the actual self-concentration calculated in the simulation, $\phi_{\mathrm{eff,\,i}}(r)$ is captured by both the LM and the SCLM set of equations. However, a careful inspection reveals that the self-consistent definition provides a more accurate description of the decay at close distances. While the above equations provide a concise formulation of the variation of the *mean* concentration as we enlarge a spherical volume centered at a PI or PS atom, certain important aspects remain. First, as discussed earlier, it has been proposed that fluctuations are important both for intermolecular neighbors as well as the self-concentration term. Second, despite extensive effort, it remains still unclear whether a single length over which these concentrations are calculated, suffices to describe dynamics. This will be further discussed in the following sections. First, we will describe how dynamics are affected by blending in our systems.

C. Local Dynamics

The segmental dynamics of the mixture were studied separately for each component. In order to compare directly to available experimental data we analyzed the second Legendre polynomial, defined as:

$$P_2^{\mathrm{CH}}(t) = \frac{3}{2}\langle \cos^2\theta(t)\rangle - \frac{1}{2} \tag{5}$$

for backbone carbon-hydrogen C-H vectors for PS and for the first carbon atom of each PI monomer following the ^{13}C labeling scheme employed in the study of He et al.[18] Orientation decorrelation dynamics were described using a modified Kohlrausch-Williams-Watts (mKWW) funtion:

$$G(t) = \alpha_{\mathrm{lib}} \exp\left(-\frac{t}{\tau_{\mathrm{lib}}}\right) + (1-\alpha_{\mathrm{lib}}) \exp\left[-\left(\frac{t}{\tau_{\mathrm{seg}}}\right)^{\beta}\right] \tag{6}$$

In Fig. 4a) we present an example of simulation data with mKWW fits for one system. It is clear that PI dynamics is quantitatively described by the above expression. For PS, some deviations were observed with the mKWW overestimating decorrelation at intermediate times and underestimating it at the long tails. Most of the data were conforming to the following parameters: τ_{lib}=0.1 ps (0.3), α_{lib}=0.3 (0.1) for PI (PS) and $\beta \approx 0.6$ (results presented in Table II). While the mKWW is only a formula to describe actual simulation data it is very instructive to discuss the values found. First, pure components present

segmental times that are significantly disparate by two orders of magnitude. Mixing alters these times, slowing the faster PI component and inducing an opposite action to PS as anticipated. It is also noteworthy that the parameter β which describes the stretching of the autocorrelation curve (or the breadth of an underlying distribution of exponential relaxation times) becomes progressively lower as we introduce more PS. Surprisingly, pure PS had a higher value of β (≈ 0.6) relative to the 25/75 %wt mixture (≈ 0.5) despite the anticipated higher T_g for PS. We acknowledge that there is substantial statistical error in these parameters (± 0.1 for β) however similar findings were reported in the experiments by He al.[18] For pure PI and the 75/25 system β was found to be 0.62 and 0.58 with a decrease to 0.52 and 0.46 for higher PS concentrations. In contrast, for PS β slightly decreased first from 0.51 to 0.49 and then it was described by 0.50. In any case, direct comparison can only be made by transforming simulation data to T_1 values.[47]

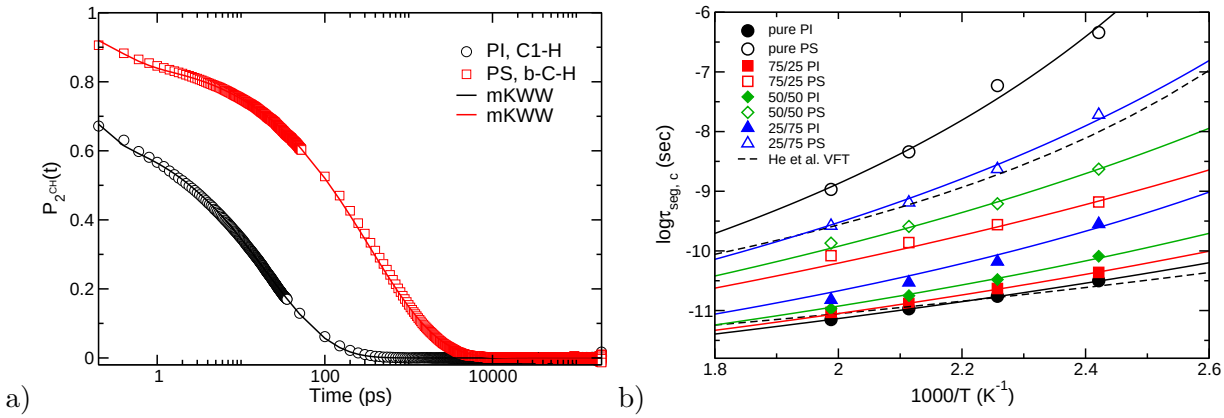

FIG. 4. a) Averaged orientation autocorrelation functions of unit vectors along carbon-hydrogen bonds (see text) for PI and PS at 443K and 50/50 %wt. Lines respresent best fits with the mKWW function. b) Mean correlation times provided by the mKWW description of simulation data (symbols, filled for PI and open for PS). Dashed lines are the VFT fits on experiments of pure systems.[18] Continuous lines are VFT representations of our data.

We now turn into a description of the coupled composition and temperature dependence of segmental dynamics. To proceed, we extracted the mean correlation time provided by the mKWW expression associated with segmental dynamics:

$$\tau_{\mathrm{seg,c}} = \frac{\tau_{\mathrm{seg}}}{\beta}\Gamma\left(\frac{1}{\beta}\right) \tag{7}$$

	PI				*PS*			
System	$\tau_{\rm lib}$ (ps)	$\alpha_{\rm lib}$	$\tau_{\rm seg}$ (ps)	β	$\tau_{\rm lib}$ (ps)	$\alpha_{\rm lib}$	$\tau_{\rm seg}$ (ps)	β
Pure								
413K	0.10	0.30	20.47	0.59	-[a]	0.23	309500	0.61
443K	0.09	0.30	11.44	0.59	-	0.27	40070	0.61
473K	0.08	0.29	6.99	0.59	-	0.27	3271	0.64
503K	0.08	0.30	4.76	0.60	-	0.27	752	0.63
75/25								
413K	0.11	0.31	27.57	0.58	0.28	0.12	400.6	0.56
443K	0.09	0.30	14.34	0.56	0.26	0.12	172.3	0.57
473K	0.09	0.30	8.46	0.58	0.32	0.13	91.32	0.60
503K	0.09	0.31	6.03	0.59	0.19	0.1	51.26	0.57
50/50								
413K	0.10	0.30	40.51	0.50	0.27	0.12	1233	0.51
443K	0.10	0.32	20.05	0.56	0.28	0.13	342.8	0.53
473K	0.09	0.30	10.34	0.54	0.34	0.14	161.3	0.57
503K	0.08	0.29	6.27	0.55	0.29	0.13	78.81	0.55
25/75								
413K	0.09	0.25	70.68	0.38	0.52	0.15	8700	0.48
443K	0.10	0.29	27.56	0.46	0.87	0.18	1319	0.54
473K	0.09	0.28	13.3	0.47	0.35	0.14	348.0	0.52
503K	0.09	0.29	7.7	0.51	0.34	0.14	146.8	0.53

[a] For pure PS we did not explicitly accounted for an initial fast decorrelation

TABLE II. Parameters extracted from modeling simulation data with the mKWW function. Error bars are about 10% of the actual values for both $\tau_{\rm seg}$ and β.

We note that $\tau_{\rm seg,c}$ is less sensitive to the choice of β than $\tau_{\rm seg}$. Fig. 4b) presents the extracted mean times from all simulations with symbols; given the logarithmic scale we expect that errors are approximately equal to symbol sizes. Nevertheless, as we will discuss further later on, these errors are significant since any attempt to characterize an appropriate lengthscale

for cooperative dynamics is extremely sensitive to the values depicted in Fig. 4b). We can quantitatively compare our results to experimental measurements represented by the dashed lines reproduced only for the pure components (for clarity). It is apparent that pure PI dynamics is captured by our model quantitatively. This is not the case for PS as mentioned in the methodology section where slower segmental dynamics are observed. Despite deviations for PS, we clearly observe a significant accelaration of the slower component and a minor deceleration of PI, a feature well-established in such blend dynamics. Continuous lines in the same figure are the results of a first attempt to employ the LM model.

The LM model correlates dynamics to different effective glass transitions $T_{\mathrm{g,\,eff}}$ experienced by individual components. To proceed with such an analysis we need data at low temperatures. Since simulations are not feasible in proximity to T_g we extract such parameters using the Vogel-Fulcher-Tammann (VFT) expression for the variation of mean segmental times with temperature:

$$\log\left(\frac{\tau_{\mathrm{seg,\,c}}}{\tau_\infty}\right) = \frac{B}{T - T_0} \tag{8}$$

where τ_∞, B and T_0 are constants that should in principle be determined independently for each component in each composition. This is an important aspect that will return to our discussion. For this section, it is clearly not practical to extract these values solely by data on four temperatures. Following the literature, we assume that B and τ_∞ are different for each component but do not change with mixing.[18] To further proceed, since we are far from T_g we assume that T_0 for each pure component is equal to the values employed in analysis of experimental data (152K and 273K for PI and PS respectively); this is preferable than adopting values for B which have larger error.[18] With these assumptions we can now *simultaneously* fit all 16 points (times) for each component using five parameters: B, τ_∞ and $T_{0,k}$ where k refers to the three mixtures (75/25, 50/50 and 25/75). We found that starting from pure PI where T_0 is kept at 152K, $T_{0,k}$ values increase to 166.9, 186.6 and 220.8K as we move to higher concentrations of PS. In contrast, for PS, starting at 273K, $T_{0,k}$ values decrease by mixing with PI with values 169.2 K, 198.3 and 231.8 for the 75/25, 50/50 and 25/75 mixtures respectively. B values extracted are 656.3 K (964.3 K) for PI (PS) respectively while τ_∞ was 0.1 ps for both polymers. The actual model VFT curves are represented in Fig. 4b) by the continuous lines. In general, the extracted curves are within the error of the data however it appears that errors are systematic, partially due

to ignoring fluctuations as we will describe in subsequent sections. The analysis allows to calculate effective glass transitions for each component i by correlating changes in $T_{0,i}$ by blending to changes in $T^i_{\mathrm{g,\ eff}}$:

$$T_{0,i}(\phi) = T_{0,i}(\phi) + [T^i_{\mathrm{g,\ eff}}(\phi) - T^i_g] \tag{9}$$

taking values of 190 K and 319 K for the pure PI and PS respectively.[18] Subsequent application of the Fox equation:

$$\frac{1}{T_{\mathrm{g,\ eff}}(\phi_{\mathrm{eff}})} = \frac{\phi_{\mathrm{eff}}}{T^{\mathrm{A}}_{\mathrm{g}}} + \frac{1-\phi_{\mathrm{eff}}}{T^{\mathrm{B}}_{\mathrm{g}}} \tag{10}$$

provides an effective concentration for each component which is our aim. The values extracted for the three mixtures for PI are 0.82, 0.62 and 0.35 (by increasing PS content). These can be directly compared to the overall bulk fraction which is 0.79, 0.56 and 0.29 (reported also in Table I). For PS, values are 0.30, 0.55 and 0.78. If we attempt to identify a cutoff radius R_c that signifies the range over which dynamics are experiencing this effective concentration using Fig. 3 we find values for PI of $\approx$ 1.3 nm (almost twice the PI Kuhn length). For PS there is a systematic trend for this range to decrease starting also from a value $\approx$ 1.3 nm down to 1 nm for the mixture with the highest PS content. Attributing this higher effective content due to self-concetrations results to a value of ϕ_{self}(PI)=0.13 while for PS ϕ_{self}(PS)=0.16-0.26. Despite the approximations introduced, it is apparent that for the slower component employing a mean effective concentration over a specific range does not suffice to capture the simulation data (Fig. 4b). We believe the same is true for PI, however closer proximity of PS to the T_g of the blend makes this effect clearer. Furthermore, while the self-concentration terms for PI in range of 1.3nm presents as the most reasonable choice in agreement with proposed values in past studies[18,27] we find that deviations in Fig. 4b) are present and their origin could be either the accumulated statistics of the simulations or an underlying defficiency of the LM model. In the next sections we examine whether introducing concentration fluctuations improves the description of blend segmental dynamics.

D. Concentration Fluctuations

The extracted values for ϕ_{eff} were correlated to a cooperative length and a value for self-concentration using mean values which only represent the first moment of a distribution of

local concentrations. Fluctuations of ϕ_{eff} could be important not only due to changes in the intermolecular environment but also due to a range of self-concentration values accessible within the same cooperative length. Liu *et al.*[21] employing a Lennard-Jones polymer model proposed that a distribution of intramolecular concentrations play a significant role across different compositions, particularly at the dilute limit. This effect becomes progressively more important as we decrease the radius R_c chosen for the cooperative length down to 1.5σ, which is approximately equal to the Kuhn segment, for the simple LJ model polymer system employed. Note that atomistic models of PMMA with intrinsic rigidity at such lengthscales present a distribution of self-concentrations with a peak at 1.[28] We will return to this discussion after briefly commenting on density fluctuations and mixing.

For the systems we studied we did not observe significant changes on the fluctuations of the self-concentration term by blending. The insets in Fig. 3c,d show that the mean values of the self-distribution between pure components and the 50/50 mixture are identical. A weak-temperature dependence emerges from the use of a fraction and the incompressibility of a single-chain that carries over to the distribution of self-concentrations normalized to the total density. These implies that the fraction of self-contacts will decrease with a temperature decrease. However, as described earlier, mixing has a minute effect on the total concentration of atoms; furthermore no changes are discerned for the self-terms or their fluctuations. Thus we conclude that to a good approximation self-concentrations are constant with regards to blending with a small temperature dependence. After the above discussion, for the remaining of this study we will employ fractions of atoms ϕ instead of number densities ρ and examine the dependance of these fluctuations as we change the cutoff radius R_c representing a selected cooperative length.

Figs. 5a,b present the distribution of effective concentrations with a decomposition to its constituents (self- and inter-) for a highly assymetric mixture (25/75 PI/PS). For these calculations, we excluded the end monomers for reasons that will be further clarified in the next section. The probability for a specific value of an effective concentration is the result of the convolution of the underlying self- and inter- terms.[19] There are several important features displayed by such an analysis. First, at large separations, fluctuations $\langle \delta\phi^2_{\text{eff}} \rangle$ were in the range of 0.1-0.2 suggesting a weakly interacting blend; $\langle \delta\phi^2 \rangle$ has been proposed to be inversely proportional to R_c,[19] however this is not straightforward to examine given the highly broad distributions as we move to shorter distances. At these shorter distances, as

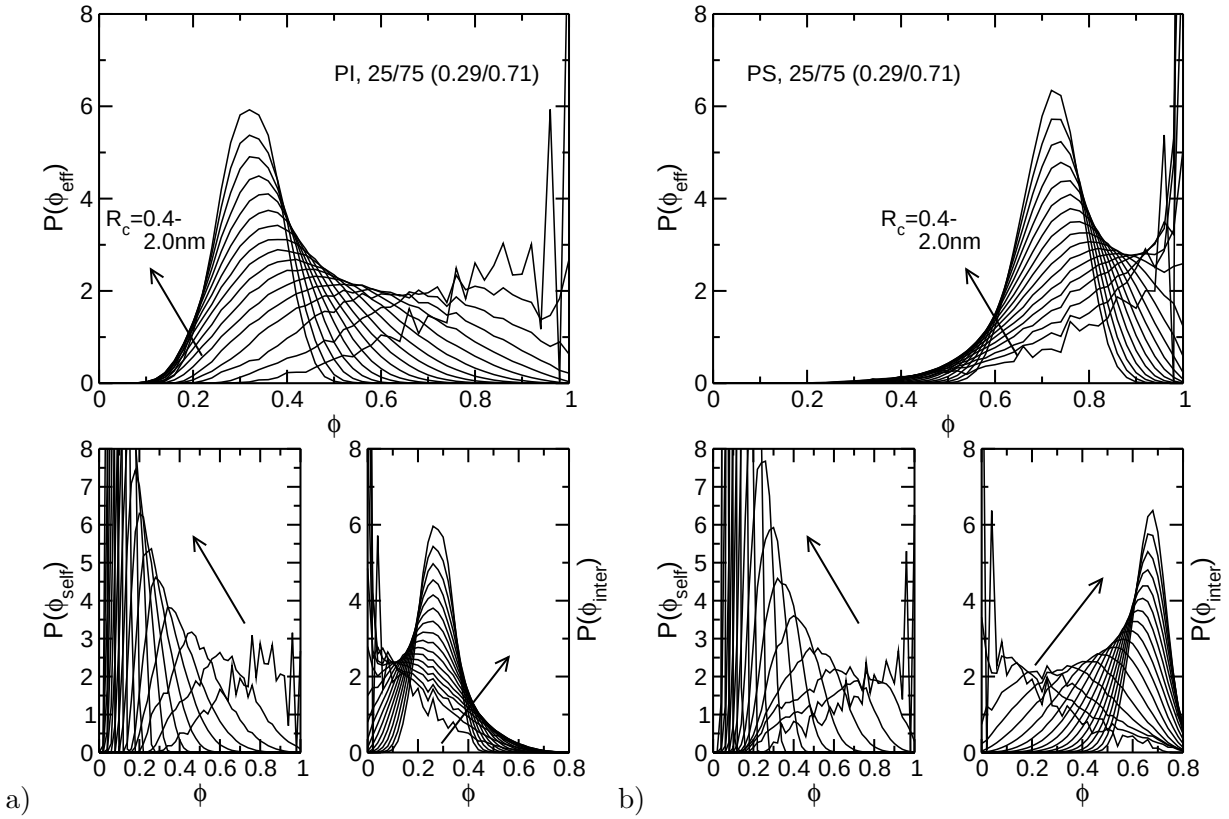

FIG. 5. a) Distribution of total and self- and inter-PI fractions around a PI atom within in a radius R_c for the 25/75 system at 443K. b) Distribution of total and self- and inter-PS fractions around a PS atom within a radius R_c for the 25/75 system at 443K. Arrows point towards increasing radii. All curves have been calculated around atoms of PI or PS, excluding the first and last monomer of each chain.

discussed by Liu et al.[21] fluctuations of the self-term become important. Note for the same R_c (i.e. 0.5 nm) the self-PS term displays a much broader distribution. This result provides evidence that PS atoms are exposed to a larger spectrum of self-concentrations which could directly enhance their exposure to the environment. Finally, at very short distances the resulting effective concentrations present a maxima at $\phi_{\rm eff} = 1$. This is an important observation that results to a further complication if we wish to introduce concentration fluctuations within the LM model. Specifically, if a single characteristic relaxation time is associated with a specific value of $\phi_{\rm eff}$ then this will result to an equivalent abrupt distribution of relaxation times. This finding was realized in past analysis of experimental data and additional broadening of the distribution of times was introduced using the empirical Havriliak-Negami function as calculated from the equivalent pure components.[19] Finally we

mention that we restricted the range of R_c examined to 0.4-2nm. Shorter distances present fluctuations with peaks probing characteristic features of the single chain intramolecular distribution function; i.e. related to the specific monomer structure (bond lengths and bond angles).

E. Distribution of relaxation times

Introducing concentration fluctuations with a probability $p(\phi_{\rm eff})$ can provide a spectrum of distribution of relaxation times $p(\log \tau_{\rm seg\ c})$. One approach would be to compare the mean $p(\log \tau_{\rm seg\ c})$ to the values reported earlier (Fig. 4b). A different, more rigorous comparison requires access to the full underlying spectrum of $p(\log \tau_{\rm seg\ c})$ probed during the simulations. CH vectors, even in pure systems, reorient with different distributions of relaxation times whose mean values are affected by the surrounding free volume; the average free volume varies as a function of position along the chain.[48] To extract an underlying distribution of times we undertook the challenge to fit each CH vector individually with a mKWW function. We should note here that this is a non-trivial statistical problem due to rather small, compared to realistic, systems studied in all atomistic MD simulations. Thus, it is not surprising that, according to our knowledge, such a detailed analysis has not been performed before in atomistic models of polymer blends. In order to improve statistics we modelled each curve using the same β, $\alpha_{\rm lib}, \tau_{\rm lib}$ extracted from the overall analysis (Table II). We relied on automating a constrained optimization scheme with the Levenberg-Marquardt algorithm as implemented in the Octave software[49] and performing thousands of such individual fits. Specifically, for PI and PI in blends we employed the 20, 200 ps short runs (initial configurations separated by $\Delta t = 10$ ns in the long trajectory) to extract the correlations of individual CH vectors (i.e. 768 for the PI in the 50/50 system which resulted to 15,360 curves). For PS in blends we calculated correlations during segments of the long trajectory (200 ns), progressively longer for lower temperatures. We note that statistics were very poor for pure PS at low temperatures; at 413K only the single whole trajectory was employed resulting to 1,680 curves. Given the limited quality of the fits, data for PS at low temperatures appeared insufficient for our analysis. Nevertheless we can circumvent this limitation by looking at the temperature dependence of the extracted distribution of $\log \tau_{\rm seg\ c}$ as described below.

Fig. 6a) presents "raw" data for pure PI at 443K; even as high as half of the points

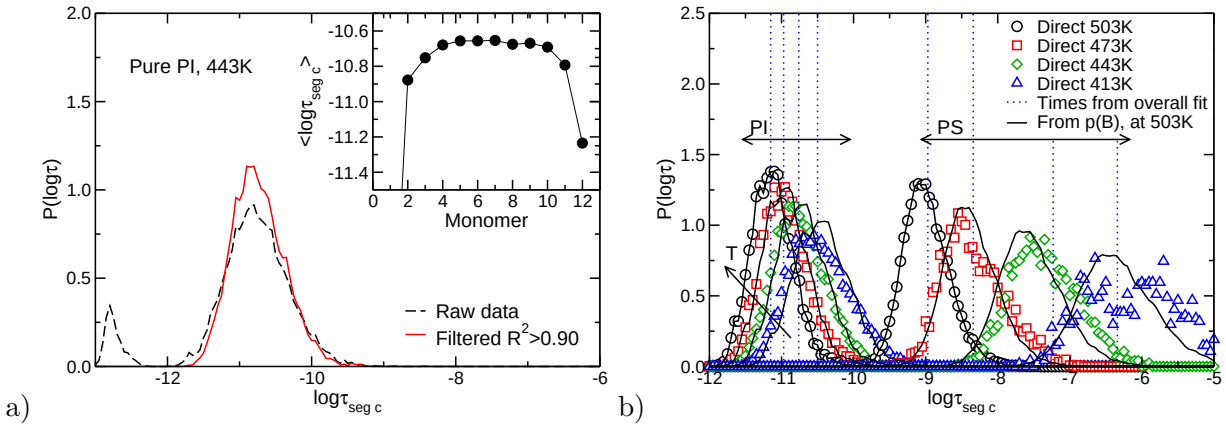

FIG. 6. a) Distribution of $\log \tau_{\text{seg c}}$ extracted for pure PI at 443K (dashed lines). The continuous line is the result after filtering out fits with correlation coefficient $R^2 < 0.95$ and removing data for vectors residing on end-monomers. The inset displays average times as a function of monomer position. b) Distribution of $\log \tau_{\text{seg c}}$ for pure PI and PS for all temperatures studied (filtered, open symbols). Dotted vertical lines represent values extracted independently by fitting the overall trajectory as reported in Fig. 4b). Continuous lines represent predictions based on the concept of an underlying distribution of T-independent activation energies extracted at 503K.

originate from curves with poor statistics that should not be analyzed further. Notice that a peak at the sub-picosecond times is present. This is the result of the fast re-orientation of CH vectors residing at end monomers as shown by the mean $\log \tau_{\text{seg c}}$ as a function of monomer position in the inset. The faster relaxation towards ends of the molecules is a direct result of the increased available free volume as we have explicitly quantified in past studies.[48] To remove results from curves with poor statistics we filtered-out the "raw" data by requiring that the correlation coefficient of the fit is higher than 0.95. Before proceeding with further analysis though, it is important to examine that setting parameters of the mKWW to the "overall" determined values and filtering-out poor fits does not bias the extracted distribution; we did not find any such evidence as shown in the same figure by the continuous and dashed lines (the different height is the result of renormalization after removal of end-monomer contributions).

It is anticipated that the distributions of $p(\log \tau_{\text{seg c}})$ will be T-dependent. However, as noted earlier, it is particularly challenging to extract such distributions for PS at low-temperatures. Therefore, we proceed under the assumption that the distribution of $\log \tau_{\text{seg c}}$

extracted at 503K for each of the pure components is the result of a distribution of T-independent activation energies introduced in the VFT formalism. Mathematically, this requires a transformation of a probability density function $p(\log \tau_{\text{seg c}}) \rightarrow p(B)$ using the VFT equation and values for T_0 and τ_∞ determined previously for the pure components. Specifically, we create a set of distinct points B_i, then we find the probability of observing $\log \tau_{\text{seg c},\, i} = B_i/(T - T_0) + \log \tau_\infty$ by spline interpolation on originally calculated data at 503K. $p(B_i)$ is given by the product $p(\log \tau_{\text{seg c},\, i})$ with $T - T_0$ as the appropriate derivative $dB/d \log \tau_{\text{seg c}}$.[50] If our assumption is reasonable then an inverse procedure can produce distributions $p(\log \tau_{\text{seg c}})$ at the remaining temperatures (413, 443, 473) which can be directly contrasted to calculated data. Fig. 6b) presents these estimates with several important features being eminent. First, by examining the open symbols (direct calculation by fitting individual CH vectors filtered as described earlier) and the vertical dotted lines (extracted by overall fits reported in Fig. 4b) we find that the extracted distributions are consistent with the mean relaxation times reported previously. The success of this approach is heavily due to the ability to automatically optimize tens of thousands of decorrelation curves and filtering out poor descriptions without biasing the resulting distributions. Second, we find that for PI, regenerating distributions based on the concept of a T-independent underlying distribution of B proves to be a rather valid approach. Third, for PS, modeled distributions are not in good agreement at low temperatures (443K and 413K). Interestingly, the predicted distribution is clearly shifted towards shorter times at 443K; note that the mean value reported in Fig. 4b exhibits a similar deviation from the VFT fits, suggesting simply that accuracy is limited due to the length of the trajectory. Finally distributions for PS at 413K are highly unreliable due to the small sample utilized; nevertheless we choose to present them to show that again, the approach with a distribution of activation energies appears to be reasonable. We conclude this discussion by stating that within the accuracy of simulations, the distribution of activation energies extracted at 503K appears to reliably model pure component dynamics at lower temperatures. Therefore, by analyzing tens of thousands of curves we can now access a distribution of relaxation times exhibited by segments of each component in the mixtures and compare to theoretical predictions using $p(\phi_{\text{eff}})$ and pure component $p(\log \tau_{\text{seg c}})$.

F. Correlation between relaxation times and effective concentration

Prior to proceeding to the effect of concentration flucutations we would like first to establish that indeed changes in effective concentrations alter dynamics. In more detail, we calculated for each hydrogen, in all CH vectors analyzed before, self-, $\phi_{\rm self}$, and effective, $\phi_{\rm eff}$, local composition for both PI and PS. Since local composition depends strongly on the actual length scale (see Fig. 3), we consider various distances from a reference H atom, R_c, from 0.4 nm up to 1.3 nm. Thus, we do have information, for each CH vector considered here (for both PI and PS), not only about its dynamical behavior (segmental relaxation time) but also about its local environment. Our goal is to check weather changes in $\phi_{\rm eff}$ of PI (or PS) alter $\tau_{\rm seg,c}$ of PI (or PS). Note, that the direct correlation of these quantities is a complex statistical problem since it involves correlation between two very noisy variables. In order to improve statistics, we are grouping together all atoms that have the same $\phi_{\rm eff}$ within a specific $\Delta\phi_{\rm eff}$ interval (here $\Delta\phi_{\rm eff}$=0.1), independently for each component. Next, we calculate for each component the average relaxation time for all CH vectors with $\phi_{\rm eff}$ in the same interval, i.e. $\tau_{\rm seg,c}(\phi_{\rm eff})$.

Data about the average relaxation time of both PI and PS, as a function of its local environment, for a specific system (50/50, T=443K) are shown in Figs. 7a and b. First, in Fig. 7a we present $\tau_{\rm seg,c}(\phi_{\rm eff})$ of PI for various local PI effective compositions, $\phi_{\rm eff}$. $\phi_{\rm eff}$ was calculated using different R_c ranging from 0.4 to 1.3 nm. It is evident that for any R_c chosen, decorrelation times of the low-T_g (PI) component, decrease with an increase of $\phi_{\rm eff}$ (or decrease of the concentration of the high-T_g component, PS, since $\phi_{\rm eff}^{PI} + \phi_{\rm inter}^{PS} = 1$). The actual functional dependence is stronger for values of R_c (0.4 nm), for which $\tau_{\rm seg,c}(\phi_{\rm eff})$ reduces by a factor of about 2.5 as $\phi_{\rm eff}$ goes from 0.7 to 1.0. For the larger distances $\tau_{\rm seg,c}(\phi_{\rm eff})$ decreases about 2 times as $\phi_{\rm eff}$ increases from 0.3 to 1.0.

Additionally, in Fig. 7b data about the average relaxation time, $\tau_{\rm seg,c}(\phi_{\rm eff})$, of PS as a function of PS effective composition are presented. As expected the relaxation time of the high-T_g (PS) component, increases as its concentration increases; i.e. its dynamics becomes slower. The dependence of PS $\tau_{\rm seg,c}(\phi_{\rm eff})$ on $\phi_{\rm eff}$ is much stronger for small length scales: for R_c=0.4 nm relaxation time increases by a factor of about 100 as $\phi_{\rm eff}$ increases from 0.5 to 1.0, whereas for R_c=1.3 nm increases by a factor of about 5. It is even more important to notice the much stronger dependence of the segmental dynamics of PS on its local environment,

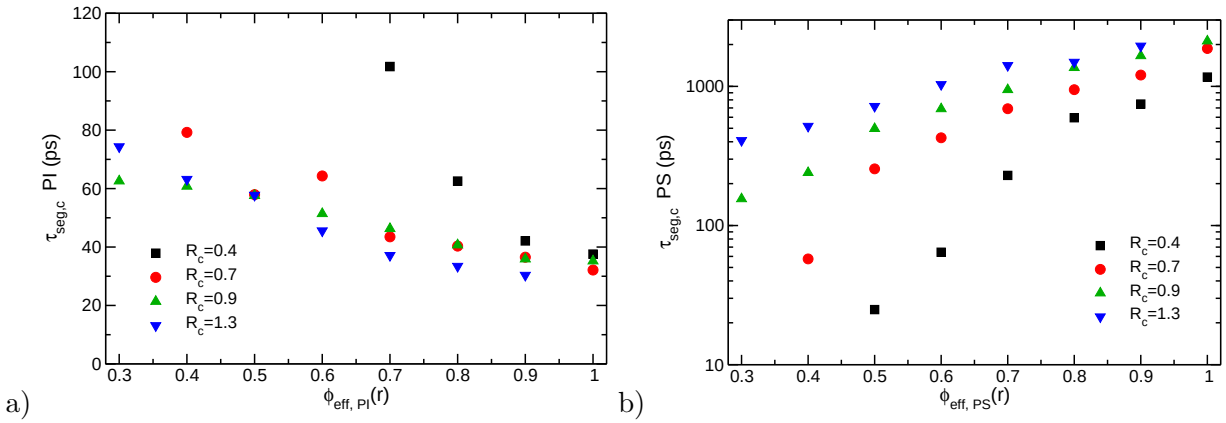

FIG. 7. a) Relaxation times of PI as a function of effective concentration calculated at different distances, R_c, from a reference PI atom. b) Relaxation times of PS as a function of effective concentration of PS calculated at different distances, R_c, from a reference PS atom. In both cases the system is the 50/50 PI/PS blend at T=443K.

compared to the case of PI discussed above. This aspect will be further discussed in the next section in accordance to the terminal dynamics. As a final remark here we should state that the monomer structure of a specific polymer plays a crucial role in the dependence of its segmental dynamics on its local environment; we believe this is related to other systems where it has been argued that intermolecular packing plays a critical role.[2,28]

G. A second approach to the LM with concentration fluctuations

Equipped with a reliable method to generate distributions of $\log \tau_{\text{seg c}}$ for the pure components and a direct calculation of $p(\phi_{\text{eff}})$ from atomistic simulations we can now re-examine the application of the LM model coupled with concentration fluctuations.[19] The procedure is analogous to calculating the probability density of a function of two variables, namely B and T_0 (where the $p(T_0)$ is derived by transformation of $p(\phi_{\text{eff}})$ using the Fox equation, Eq. 10) and requires calculation of the appropriate Jacobian.[50] This process was performed iteratively for different R_c (from 0.4 nm to 2 nm using a step of 0.1nm) and the extracted $p(\log \tau_{\text{seg c}})$ can be rigorously compared to the directly calculated. A unique feature of our strategy, is that simulations provide direct information on $p(\phi_{\text{eff}})$ and fluctuations associated with this parameter. Therefore no assumptions for the structure of the mixtures are made. To be consistent with the distribution of times extracted, concentrations were calculated

starting from PI or PS atoms that did not belong to end-monomers as shown in Figs. 5a,b; however, we note that we did not find any significant effect on the overall averaged distribution of effective concentrations.

We calculated distributions for radii ranging from 0.4-2.0 nm and compared to directly extracted spectra of relaxation times. The optimum radius for each set of data was selected based on the Kolmogorov-Smirnov test for the cumulative probability density function.[51] Results for two temperatures are synopsized in Figs. 8a) and b). Overall, allowing a variable cooperative length provides a satisfactory description, especially when the errors involved in the data extracted are considered. We found that incorporating concentration fluctuations provides a lower value for PI that ranges between 0.6-0.4 nm in agreement to experimental studies.[19] In contrast for PS a longer distance from 0.9-1.5 nm was obtained. This length scale for PI is consistent with a length close to it Kuhn segment, whereas for PS (oligomer) is smaller than its Kuhn segment. In addition, the values were systematically decreasing for PI and increasing for PS with temperature rendering the model unsatisfactory. One significant (but necessary) assumption that can contribute to this effect is the adoption of T_g equal to reported data from experiments. Finally, we should also note here that in a previous dielectric relaxation spectroscopy study of PI/PS oligomer blends[6] it was shown that a model, which incorporates only concentration fluctuation effects described through mean-field approximation,[4] predicts the dynamics of PI if a dynamic correlation length of about 1.48 nm is being used. This value further enhances the importance of both self-concentration and concentration fluctuation effects in the relaxation of PI.

Despite the previously mentioned approximations, our study provides further insight into deviations from the theoretical model. A surprising feature observed, is that for PI the distribution of times becomes narrower for the system with the lowest PS content and then broadens as more PS is added. For the 75/25 system at 443K, a radius less than 0.4 nm would probably capture the mean value in better agreement; nevertheless as noted earlier such values render non-continuous effective concentrations. This is in contrast to the slow component, where an extreme breadth is found for relaxation times in the 25/75 prior to narrowing as we increase PI concentration. It appears therefore that the change in the width of the distributions is somewhat coupled; to the best of our knowledge this can not be reproduced for PI while maintaining high effective concentration corresponding to a T_g close to the pure state. Mathematically, it is straightforward to recognize that our

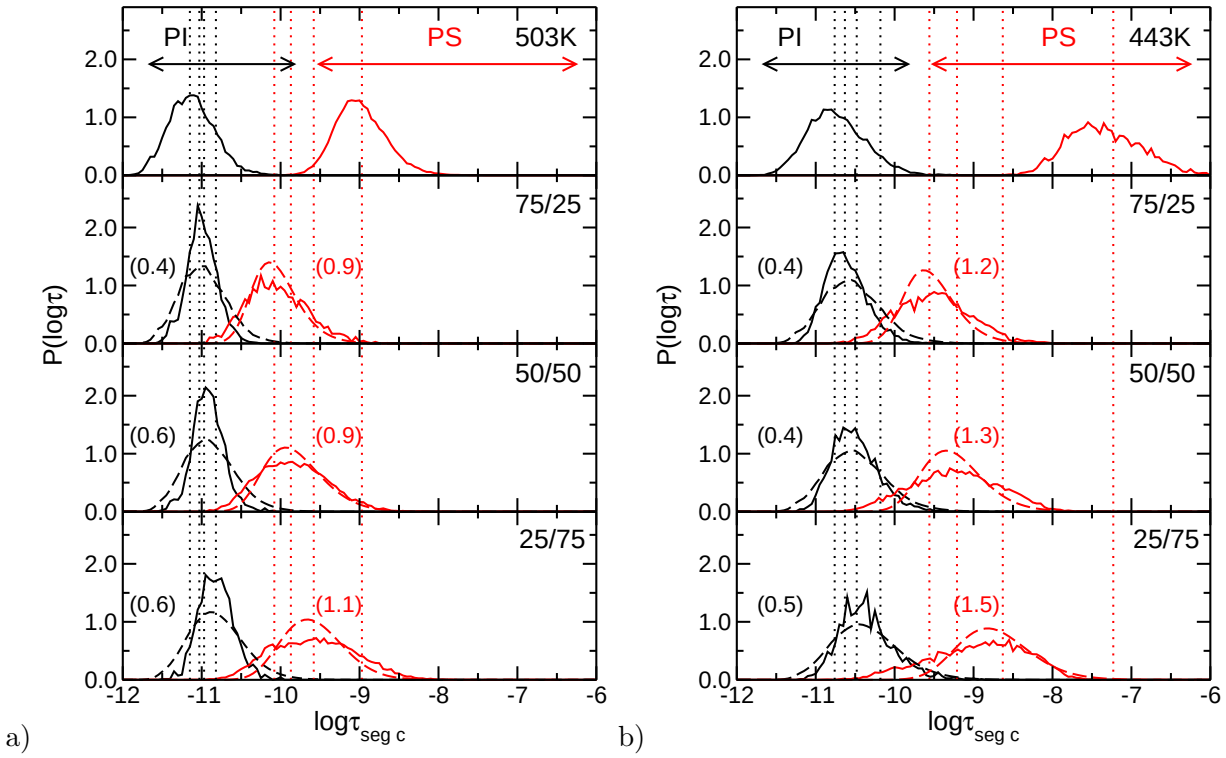

FIG. 8. a) Distribution of relaxation times measured at 503K as a function of blend composition for each of the two components. The vertical dashed lines correspond to the times reported in Fig. 4b for each system. Dashed lines, depict optimum fits for the distribution using the LM-concentration fluctuations model and effective concentrations calculated from simulations. Values in parentheses denote the corresponding cutoff radius. b) Same as a) for 443K.

procedure employed the underlying assumption of independency between the two variables that produce the distribution $p(\log \tau_{\text{seg c}})$, namely T_0 and B. As stated earlier, a similar approach is used when modeling experimental data using a distribution function originating from the pure component.[19] We believe that more accurate descriptions could be provided to the model if concentration-dependant activation energies are employed. However, to the best of our knowledge, there is currently no framework to provide mixing rules for such activation energies.

IV. TERMINAL-CHAIN DYNAMICS

A. Translational dynamics

In the last part of this work we present data about the global chain dynamics. In the experimental study of He *et al.*, diffusion coefficients D for the two components were found approximately equal based on a unimodal description that would fail if these parameters differ more than a factor of 3.[18] Data about D_{PI} and D_{PS} of all blends as well as of pure components directly calculated from our simulations are shown in Fig. 9. The strong dependence of diffusion coefficients on T, particular of D_{PS} is evident. Furthermore, in the same figure we also present results from NMR measurements of PI/PS oligomers blends by He *et al.*.[18] D for pure PI, D_{PI} is in quantitative agreement with the experimental data at all Ts studied herein. On the contrast, for pure PS, D_{PS} are only in qualitative agreement with the experimental data; i.e. the specific all-atom PS model predicts slower, compared to experimental data, dynamics as it has also reported and discussed extensively in the past.[37,52]

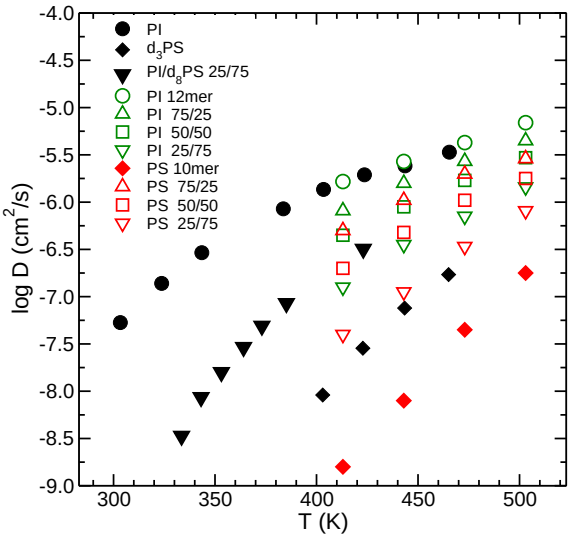

FIG. 9. Diffusion coefficient of all model systems studied here (open symbols). With full symbols are experimental data from the literature.[18]

More important is the composition dependance of the dynamics of the two components in the blends. As expected as the concentration of the low-T_g, component (PI) increases

D of the low-T_g, component decreases, whereas for the high-T_g, component (PS) increases, compared to their bulk (pure component) values. It is noticeable that as the concentration of PI increases the difference between the diffusion coefficients of the two components becomes progressively smaller: for pure components D_{PS} is about two orders of magnitude larger than D_{PI}, whereas for the PI/PS 75/25 blends D_{PS} is only 2-3 times D_{PI}. Thus, in agreement to experimental data, diffusion appears to be similar for the components albeit not exactly equal. This strong coupling between the friction coefficients of the two components is not surprising if we consider that: (a) First, model blends studied here are rather oligomers, with a molecular length clearly below the Rouse regime. For simple molecular systems (e.g. Lennard-Jones liquids) it is clear that similar diffusion coefficients are expected for both components. (b) Second, of particular importance are the length scales involved in the dynamics of the model systems. Both PI and PS have rather similar backbone lengths (as well as radius of gyration: about 0.84 nm for the 12-mer PI and 0.7 nm for the 10-mer PS) that experience on the average the same environment. Therefore it is reasonable to conclude that chain dynamics are slaved to the collective mobility occuring over these length scales in the blend. Clearly this effect will depend on the relevant size of the chains as well as on the onset of entanglements which is much different for the two components. This will be the subject of future work.

B. Orientational dynamics

In the next stage, in order to further analyze the terminal dynamics of the polymer chains we study the orientational motion of both components. In more detail, we calculated the average autocorrelation function of a unit vector along the end-to-end distance , defined, for each component i through:

$$u(t)_i = \frac{\langle R(t)_i R(0)_i \rangle}{\langle R^2 \rangle_{0,i}}. \tag{11}$$

In the above relation $R(t)$ and $R(0)$ is the end-to-end vector at time t and 0 respectively and $< R^2 >_0$ is the equilibrium average end-to-end distance. Decorrelation times were obtained again by the integral of an optimum description using a modified mKWW relation. Note that the reported relaxation times do not include very fast (short time) relaxation processes. In addition the stretching exponent of the KWW fits, β, for all systems has a

value between 0.9-0.98. Therefore, a fit in the long-time end regime of these curves with a single exponential does not alter significantly the derived relaxation times.

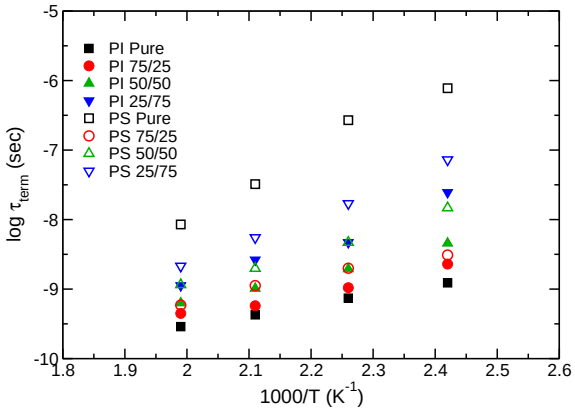

FIG. 10. Terminal relaxation time of PI (filled symbols) and PS for all systems studied here (open symbols).

Data about the terminal relaxation time $\tau_{\rm term}$ for both PI and PS are shown in Fig. 10 as a function of T for all systems studied here. In agreement with the behavior of the diffusion coefficient, discussed above, we observe strong dependence of $\tau_{\rm term}$ on T, particular for PS as well as a large difference between the terminal relaxation times for the two components: $\tau_{\rm term,PS}$ is about 2-3 orders of magnitude larger than $\tau_{\rm term,PI}$ as T varies from 503K to 413K.

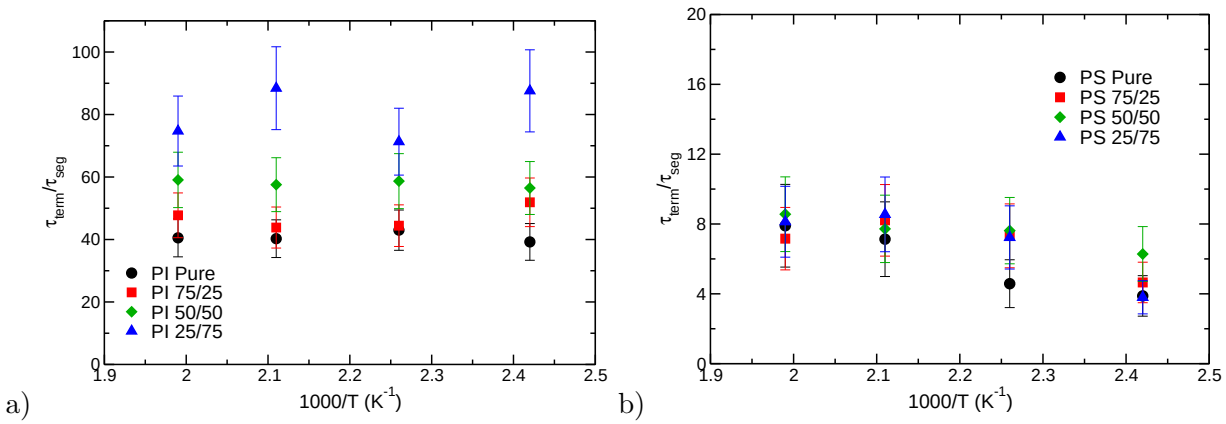

FIG. 11. Ratio of terminal to segmental relaxation time for all systems studied here. a) PI b) PS.

It is instructive to examine the ratio of terminal to segmental dynamics. As it has been observed in the past this ratio for various polymers is constant, independent of temperature,

for temperatures far away T_g.[53] Here, since we have data for both segmental and terminal characteristic relaxation times this ratio is directly accessible. In Figs. 11a and b we present the ratio $\tau_{\rm term}/\tau_{\rm seg,c}$ for all (blends and pure) systems, for PI and PS respectively. In agreement with the experimental observations we do observe that the ratio is almost temperature independent for all systems. However, there is a clear qualitative difference between PI and PS, concerning their behavior in the blends. In more detail, for the latter (PS, Fig. 11b) the ratio $\tau_{\rm term}/\tau_{\rm seg,c}$ is almost constant, independent of the composition of the blend and very similar to the ratio of the bulk pure PS. This means that both segmental and terminal dynamics of PS are similarly affected by blending therefore changes in local friction carry over to the observed global dynamics. On the contrary, the ratio $\tau_{\rm term}/\tau_{\rm seg,c}$ for PI (Fig. 11a) depends strongly on the composition of the blend. As we increase the concentration of PS $\tau_{\rm term}/\tau_{\rm seg,c}$ increases: for the pure PI the ratio is about 40, whereas for the blend with the less PI studied here (25/75 system) is two times larger. Therefore, the terminal dynamics is affected to a larger degree than the segmental dynamics with blending; i.e. the terminal relaxation time of PI increases more than its segmental relaxation time, as the concentration of PS increases, resulting into a larger terminal/segmental ratio. The observed behavior is in agreement to the discussion presented in the previous section, where it was shown that the distribution of the segmental relaxation times for PI is not largely affected by blending. In order to better clarify this aspect we should again consider the various length scales involved in the dynamics of the two components. As mentioned above the relevant length for the segmental dynamics of PI is about 0.4-0.6 nm (see Fig. 8a) smaller than its chain dimensions (radius of gyration is about 0.84 nm), that is expected to be the relevant scale for terminal dynamics. On the contrast for PS both length scales are almost the same: the segmental dynamics is characterized by a longer distance from 0.9-1.5 nm (see Fig. 8b), whereas its radius of gyration is about 0.7 nm. Therefore, it is expected that since the segmental dynamics of PS is determined by a smaller length scale it will also be less sensitive to blending, as smaller distances are dominated by the self-composition term. In order to further examine this hypothesis a detailed study for various molecular lengths and different systems needed. This is the subject of current ongoing work.[54]

V. CONCLUSIONS

We revisited the dynamics of miscible PI/PS oligomer blends by detailed atomistic molecular dynamics simulations. Our main goal was to provide a direct link between molecular parameters and dynamical behavior of both PI and PS components in the blends using recently proposed concepts of coupled concentration fluctuation effects with enrichment due to chain-connectivity. The analysis of the atomistic simulations was performed by a comprehensive statistical approach that involves independent fits over thousands autocorrelation functions of CH vectors for each component. This method allowed us to directly access the underlying distribution of relaxation times providing unique information from detailed all-atom MD simulations for the first time to the best of our knowledge. In the next stage the local environment was considered by calculating the self-, $\phi_{\rm self}$, and effective, $\phi_{\rm eff}$, local composition for each vector at various length scales. Then a direct coupling between the local environment for a specific CH vector, at different length scales, and its actual segmental relaxation time was performed.

Overall, the main findings of the present work can be summarized as follows:

(a) Segmental dynamics of both components is strongly affected by blending. However there is a clear qualitative difference in the behavior of the two components. In more detail, for PI the distribution of times becomes initially narrower for the system with the lowest PS content and then broadens as more PS is added. This is in contrast to the slow component (PS), where an extreme breadth is found for relaxation times in the 25/75 system prior to narrowing as we increase PI concentration.

(b) There is a clear correlation between segmental dynamics of a component and its local environment for both PI and PS. Segmental relaxation times as a function of effective composition, $\tau_{\rm seg,c}(\phi_{\rm eff})$, were calculated at different distances: 0.4 nm, 0.7 nm, 0.9 nm and 1.3 nm. For all lengths, the relaxation time of both components decreases as the concentration of the low-T_g (PI) component increases; the dependence of the relaxation time on the actual values of $\phi_{\rm eff}$ being much stronger for the shorter distances. Most importantly a stronger dependence of the segmental dynamics of PS on its local environment, compared to the case of PI was found.

(c) Chain dynamics of both components in the blend were quantified by calculating directly diffusion coefficients and orientational autocorrelation functions. As expected, as

the concentration of the low-T_g, component (PI) increases the diffusion coefficient of the low-T_g, component decreases, whereas the diffusion coefficient of the high-T_g, component (PS) increases, compared to their bulk (pure component) values. Strong coupling between the friction coefficients of the two components was found that leads to very similar chain dynamics for PI and PS, particularly for blends with high concentration of PI. We attribute this finding to the rather short oligomers (below the Rouse regime) studied here, as well as, to the rather similar size of PI and PS chains.

(d) Terminal dynamics were further examined by calculating the maximum relaxation time of chain, defined through the modified KWW description. A large difference between the terminal relaxation times for the two components was observed: $\tau_{\mathrm{term,PS}}$ was predicted to be 2-3 orders of magnitude longer than $\tau_{\mathrm{term,PI}}$ as T varies from 503K to 413K. The ratio of the terminal to the segmental relaxation time, $\tau_{\mathrm{term}}/\tau_{\mathrm{seg,c}}$, presents a clear qualitative difference for the two components: for PS it remains approximately constant, independent of the composition of the blend and very similar to the ratio of the bulk pure PS. On the contrary, for PI this ratio depends strongly on the composition of the blend; i.e. the terminal relaxation time of PI increases more than its segmental relaxation time, as the concentration of PS increases, resulting to a larger terminal/segmental ratio. We provide a rationale of this finding based on the different length scales characterizing dynamics. The relevant length for the segmental dynamics of PI is about 0.4-0.6 nm, smaller than chain dimension which is expected to be the relevant scale for terminal dynamics; in contrast for PS these length scales are similar.

As a final remark, we should state that the specific monomer structure of a polymer can play a crucial role in the hypothesis described above, concerning the controlling length scale characterizing the segmental dynamics of a polymer, as well as the terminal to segmental dynamics ratio. Therefore, to obtain further insight into the role of molecular parameters on the dynamics of miscible polymer blends, data from detailed atomistic simulations of a series of polymers with distinct chemical architectures and disparate molecular lengths are needed. This will be the subject of further ongoing work.[54]

VI. ACKNOWLEDGEMENTS

We are grateful to the University of Houston Research Computing Center for the generous allocation of computational time throughout the course of this study. VH acknowledges partially support by the European Union's Seventh Framework Programme (FP7-REGPOT-2009-1) project Archimedes Center for Modeling, Analysis and Computation under grant agreement n 245749. M.D. acknowledges financial support by the National Science Foundation under Grant No. CBET 1067356.

REFERENCES

[1]M. Doxastakis, M. Kitsiou, G. Fytas, D. N. Theodorou, N. Hadjichristidis, G. Meier, and B. Frick, J. of Chem. Phys. **112**, 8687 (2000).

[2]J. K. Maranas, Curr. Opin. Colloid and Interf. Sci. **12**, 29 (2007).

[3]J. Colmenero and A. Arbe, Soft Matter **3**, 1474 (2007).

[4]A. Zetsche and E. Fischer, Acta Polymerica **45**, 168 (1994).

[5]G. Katana, E. W. Fischer, T. Hack, V. Abetz, and F. Kremer, Macromolecules **28**, 2714 (1995).

[6]A. K. Rizos, G. Fytas, and A. N. Semenov, J. Chem. Phys. **102**, 6931 (1995).

[7]S. K. Kumar, R. H. Colby, S. H. Anastasiadis, and G. Fytas, J. Chem. Phys. **105**, 3777 (1996).

[8]S. Kamath, R. H. Colby, S. K. Kumar, K. Karatasos, G. Floudas, G. Fytas, and J. E. L. Roovers, J. Chem. Phys. **111**, 6121 (1999).

[9]S. Salaniwal, R. Kant, R. H. Colby, and S. K. Kumar, Macromolecules **35**, 9211 (2002).

[10]S. Kamath, R. H. Colby, and S. K. Kumar, Macromolecules **36**, 8567 (2003).

[11]R. Kant, S. K. Kumar, and R. H. Colby, Macromolecules **36**, 10087 (2003).

[12]S. Y. Kamath, R. H. Colby, and S. K. Kumar, Phys. Rev. E **67**, 010801 (2003).

[13]G. D. Smith and D. Bedrov, Eur. Polym. J. **42**, 3248 (2006).

[14]D. Bedrov and G. D. Smith, Macromolecules **39**, 8526 (2006).

[15]G. D. Smith and D. Bedrov, J. Polym. Sc. B **45**, 627 (2007).

[16]G.-C. Chung, J. A. Kornfield, and S. D. Smith, Macromolecules **27**, 5729 (1994).

[17]T. P. Lodge and T. C. B. McLeish, Macromolecules **33**, 5278 (2000).

[18]Y. He, T. R. Lutz, M. D. Ediger, M. Pitsikalis, N. Hadjichristidis, and E. D. von Meerwall, Macromolecules **38**, 6216 (2005).

[19]S. Shenogin, R. Kant, R. H. Colby, and S. K. Kumar, Macromolecules **40**, 5767 (2007).

[20]S. K. Kumar, S. Shenogin, and R. H. Colby, Macromolecules **40**, 5759 (2007).

[21]W. Liu, D. Bedrov, S. K. Kumar, B. Veytsman, and R. H. Colby, Phys Rev Lett **103**, 037801 (2009).

[22]R. H. Colby and J. E. G. Lipson, Macromolecules **38**, 4919 (2005).

[23]R. P. White, J. E. G. Lipson, and J. S. Higgins, Macromolecules **45**, 1076 (2012).

[24]M. Brodeck, F. Alvarez, A. J. Moreno, J. Colmenero, and D. Richter, Macromolecules **43**, 3036 (2010).

[25]S. Arrese-Igor, A. Allegria, A. J. Moreno, and J. Colmenero, Macromolecules **44**, 3611 (2011).

[26]M. Brodeck, F. Alvarez, J. Colmenero, and D. Richter, Macromolecules **45**, 536 (2012).

[27]R. Faller, Macromolecules **37**, 1095 (2004).

[28]J. Sacristan, C. Chen, and J. K. Maranas, Macromolecules **41**, 5466 (2008).

[29]R. Faller, F. Müller-Plathe, M. Doxastakis, and D. Theodorou, Macromolecules **34**, 1436 (2001).

[30]R. Faller and D. Reith, Macromolecules **36**, 5406 (2003).

[31]M. Doxastakis, V. G. Mavrantzas, and D. N. Theodorou, J Chem Phys **115**, 11339 (2001).

[32]M. Doxastakis, V. G. Mavrantzas, and D. N. Theodorou, J. Chem. Phys. **115**, 11352 (2001).

[33]M. Rubinstein and R. H. Colby, *Polymer Physics* (Oxford University Press, Oxford, 2003).

[34]F. Muller-Plathe, Macromolecules **29**, 47824791 (1996).

[35]V. A. Harmandaris, N. P. Adhikari, N. F. A. van der Vegt, and K. Kremer, Macromolecules **39** (2006).

[36]V. A. Harmandaris, D. Reith, N. F. A. Van der Vegt, and K. Kremer, Macrom. Chem. and Phys. **208** (2007).

[37]V. A. Harmandaris, G. Floudas, and K. Kremer, Macromolecules **44**, 393 (2011).

[38]D. Fritz, V. A. Harmandaris, K. Kremer, and N. F. A. van der Vegt, Macromolecules **42** (2009).

[39]V. A. Harmandaris and K. Kremer, Macromolecules **42**, 791 (2009).

[40]V. A. Harmandaris and K. Kremer, Soft Matter **5**, 3920 (2009).

[41]B. Hess, C. Kutzner, D. van der Spoel, and E. Lindahl, J. Chem. Theory Comput. **4**, 435 (2008).

[42]D. Van Der Spoel, E. Lindahl, B. Hess, G. Groenhof, A. E. Mark, and H. J. C. Berendsen, J. Comput. Chem. **26**, 1701 (2005).

[43]G. Bussi, D. Donadio, and M. Parrinello, J. Chem. Phys. **126**, 014101 (2007).

[44]U. Essmann, L. Perera, M. L. Berkowitz, T. Darden, H. Lee, and L. G. Pedersen, J. Chem. Phys. **103**, 8577 (1995).

[45]B. Hess, J. Chem. Theory Comput. **4**, 116 (2008).

[46]J. E. G. Lipson and S. T. Milner, Journal of Polymer Science Part B: Polymer Physics **44**, 3528 (2006).

[47]M. Doxastakis, D. N. Theodorou, G. Fytas, F. Kremer, R. Faller, and F. Müller-Plathe, J. of Chem. Phys. **119**, 6883 (2003).

[48]V. A. Harmandaris, M. Doxastakis, V. G. Mavrantzas, and D. N. Theodorou, J. of Chem. Phys. **116**, 436 (2001).

[49]J. W. Eaton, D. Bateman, and S. Hauberg, *GNU Octave Manual Version 3* (Network Theory Limited, 2008).

[50]B. A. Ogunnaike, *Random Phenomena: Fundamentals of Probability and Statistics for Engineers* (CRC Press, Boca Raton, 2010).

[51]W. H. Press, S. A. Teukolsky, W. T. Vetterling, and B. P. Flannery, *Numerical Recipes: The Art of Scientific Computing*, 3rd ed. (Cambridge University Press, New York, 2007).

[52]V. A. Harmandaris, N. P. Adhikari, N. F. A. van der Vegt, K. Kremer, B. A. Mann, R. Voelkel, H. Weiss, and C. Liew, Macromolecules **40** (2007).

[53]D. Yifu and A. P. Sokolov, Macromolecules **39**, 3322 (2006).

[54]M. Doxastakis and V. Harmandaris, to be submitted.